Stability of a pair of co-rotating vortices with axial flow

Clément Roy,[1,a)] Nathanaël Schaeffer,[1,b)] Stéphane Le Dizès,[1] and Mark Thompson[2]
[1]*Institut de Recherche sur les Phénomènes Hors-Équilibres (IRPHÉ), 49 Rue Frédéric Joliot-Curie, BP 146, 13384 Marseille Cedex 13, France*
[2]*Fluids Laboratory for Aeronautical and Industrial Research (FLAIR), Department of Mechanical Engineering, Monash University, Clayton 3800, Australia*

(Received 9 December 2007; accepted 12 May 2008; published online 8 September 2008)

The three-dimensional linear temporal stability properties of a flow composed of two corotating q-vortices (also called Batchelor vortices) are predicted by numerical stability analysis. As for the corresponding counter-rotating case, when the axial flow parameter is increased, different instability modes are observed and identified as a combination of resonant Kelvin modes of azimuthal wavenumbers m and $m+2$ within each vortex. In particular, we show that the sinuous mode, which is the dominant instability mode without axial flow, is stabilized in the presence of a moderate axial flow. Different types of mode with a large amplitude in the critical layer are also identified. For small separation distances (above the merging threshold), unstable eigenmodes, corresponding to axial wavenumbers that cannot be easily identified with simple resonant interactions of Kelvin modes, are also observed. Their growth rate is a substantial fraction of the growth rates of low-order resonant modes. The effects of the Reynolds number and vortex separation distance on the growth rate parameter map are considered. Finally, we analyze the similarities and differences between the stability characteristics of co- and counter-rotating vortex pairs. © *2008 American Institute of Physics*. [DOI: 10.1063/1.2967935]

I. INTRODUCTION

Large commercial aircrafts are known to create multiple trailing-vortex systems. These vortices can induce large turning moments on an aircraft following, which can be particularly dangerous during takeoff and landing. Given that the vortex strength scales with aircraft size, the imminent introduction of several new and much larger passenger aircrafts means that this problem is worsening over time and must be explicitly taken into account in air-traffic scheduling. From a purely scientific point of view, the component vortices take part in a complex dynamical evolution including merging, and the end result is generally a pair of counter-rotating vortices in the far wake. The two corotating vortices generated by the tip of the wing and the outer flap constitute the prototype vortex system, which provides one motivation for the analysis presented here, although the focus of this study is mainly theoretical. The goal is to provide the three-dimensional instability characteristics when the two vortices are identical corotating q-vortices (or Batchelor vortices[1]) including axial flow in their cores.

The two-dimensional (2D) large Reynolds number dynamics of corotating vortex pairs is now well understood. When the vortices are far apart, their dynamics is well described by the point vortex approach;[2] the two vortices remain in equilibrium with each other, and their cores are elliptically deformed owing to the strain field induced by the other vortex.[3] When they are positioned closer to each other, equilibrium is no longer possible and the two vortices merge to form a single vortex (e.g., Ref. 4). When the Reynolds number is large, the 2D dynamics is affected by the development of three-dimensional instabilities. Meunier and Leweke[5] observed experimentally that a sinuous deformation of each vortex core develops and modifies the merging process. This instability is due to the elliptic character of the streamlines and has been observed in several other systems (see Ref. 6 for a review and references therein). A model has been developed for a vortex pair without axial flow by Le Dizès and Laporte.[7] It was demonstrated that the sinuous deformation corresponds to the resonant combination of two stationary Kelvin modes of azimuthal wavenumbers $m=1$ and $m=-1$. Subsequently, the effect of axial flow on counter-rotating vortices was analyzed by Lacaze *et al.*[8,9] Lacaze *et al.*[9] considered a pair of counter-rotating Batchelor vortices. They demonstrated that other instability modes with different azimuthal and temporal characteristics were excited when axial flow was added. They were able to show that each instability mode corresponds to a resonant combination of two Kelvin modes of azimuthal wavenumbers m and $m+2$.

This work naturally follows on from that investigation of the stability of a pair of equistrength counter-rotating vortices;[9] however, it extends that analysis in a number of ways. First, the choice of corotating vortices means that the individual vortices undergo rotation about their centroid rather than the pure self-induced translation of the counter-rotating case. The addition of the associated centrifugal/Coriolis terms to the equations of motion complicates the theoretical stability analysis considerably, which is yet to be completed. The present paper investigates the problem using numerical stability analysis and explicitly studies the effect

a)Electronic mail: clement.roy@irphe.univ-mrs.fr.
b)Present address: Laboratoire de Géophysique Interne et Technophysique (LGIT), 1381 rue de la Piscine Saint Martin d'Heres, 38041 Grenoble Cedex 9, France.

of these terms on the stability characteristics. Second, while the theoretical analysis focuses on the resonance between particular pairs of Kelvin modes, at moderate strain rates, most of the wavenumber–axial flow parameter space leads to positive growth; this aspect was not explored. In particular, as pointed out by Lacaze *et al.*,[9] the theoretical analysis does not take into account the deviations from ellipticity of the vortices or the presence of the hyperbolic point between the two vortices, which is automatically accounted for by the numerical stability analysis. Surprisingly, the background growth rate can be almost as high as the growth rate corresponding to identifiable resonant interactions. Third, modes with substantial amplitude in the critical layer are identified.

II. FORMULATION

A. Base flow

The formulation mainly follows the numerical part of Ref. 9, except that here, we consider corotating vortices instead of counter-rotating vortices. We take as the base flow the z-independent flow obtained from the 2D interaction of two corotating Batchelor vortices. Each Batchelor vortex taken alone is a solution of the Navier–Stokes equations. Its axial velocity and axial vorticity can be written in cylindrical coordinates as

$$\omega_z = \frac{\Gamma}{\pi a^2} e^{-(r/a)^2}, \quad U_z = \frac{\xi a_0^2}{a^2} e^{-(r/a)^2}, \tag{1}$$

where the circulation Γ, the axial velocity strength ξ, and the initial core radius a_0 are constants. The radius $a(t)$ evolves owing to viscous diffusion according to

$$a(t) = \sqrt{4\nu t + a_0^2}, \tag{2}$$

where ν is the kinematic viscosity.

The sum of two corotating Batchelor vortices is not a solution. As explained by Le Dizès and Verga,[3] in the 2D dynamics, there is first a rapid relaxation process during which each vortex equilibrates with the other. In the frame rotating at the angular speed of the vortex pair, a quasisteady solution is reached, which subsequently slowly evolves due to viscous diffusion. As long as the system is far from the merging threshold ($a/b < 0.23$), the two vortices remain separated by a constant distance b and rotate around each other at a constant angular speed $\Omega = \Gamma/(\pi b^2)$. Each vortex also feels the strain field induced by the presence of the other one. Its streamlines are deformed elliptically at leading order and this makes each vortex sensitive to the elliptic instability. The 2D simulation is necessary to obtain a correct estimate of the strain field within each vortex. In particular, as noted by Le Dizès and Verga,[3] the strain rate at the vortex center is twice as large as that obtained from summing the contributions from the two separate Gaussian vortices. What is remarkable is that after the relaxation process (and before merging), the vortex system is mainly characterized by a single parameter a/b, where the vortex radius a evolves according to Eq. (2), as predicted for a single vortex.

The presence of axial flow does not modify these results because the axial flow and axial vorticity dynamics decouple. Moreover, as the axial flow satisfies the same advection-diffusion equation, it remains proportional to the axial vorticity during the whole 2D evolution. In practice, we perform the 2D simulation without axial flow and then add, after the completion of the relaxation process, an axial velocity component such that $U_z(x,y) = (aW_0/2)\omega_z(x,y)$.

After the relaxation period, the radius of each vortex has slightly evolved. It is this new value of a that is taken as the characteristic length scale for the stability analysis. The base flow is then characterized by three parameters, a/b, W_0, and the Reynolds number $\mathrm{Re} = \Gamma/\nu$, although the base flow is mainly independent of this last parameter.

We shall consider a continuous range of W_0 between 0 and 0.6 for three couples of parameters, ($\mathrm{Re} = 14\,000$, $a/b = 0.14$), ($\mathrm{Re} = 14\,000$, $a/b = 0.18$), and ($\mathrm{Re} = 31\,400$, $a/b = 0.168$), and provide some selected results for a few other combinations. For these values of W_0, the Batchelor vortex can be considered as stable. Weakly unstable center modes exist, but their growth rates are so small (see Ref. 10) that they never become dominant over the elliptic instability mode.

B. Perturbation analysis

The stability of the base flow obtained from the 2D simulation is examined by considering the problem in the frame rotating with the vortices and for which the base flow is quasistationary. In this rotating frame, the Navier–Stokes equations including all the Coriolis terms are linearized around the base flow. In addition, the weak diffusion of the base flow is suppressed by freezing the base flow. As the base flow is assumed to be homogeneous in the axial direction and because the perturbation equations are linear and independent of z for the axial derivatives, the axial dependence can be represented as a Fourier series. Linearity allows the stability of each wavelength, $\lambda = 2\pi/k$, to be determined separately. In practice, for a given axial wavelength, the perturbation equations are integrated in time with a random field as an initial condition. The characteristics of the most unstable mode are obtained by integrating for a sufficiently long time. For each set of base flow parameters and each wavenumber k, we obtain the growth rate, the rotation frequency, and the spatial structure of the most unstable mode.

C. Numerical codes

Two different numerical codes have been used. The first one was used for a similar study of counter-rotating vortices by Lacaze *et al.*[9] It is based on a high-order spectral-element technique, which has been described by Thompson *et al.*[11] and applied to various related problems (e.g., Refs. 12 and 13). The same code parameters and simulation domain as in Ref. 9 are used here.

The second code has been developed for the present study and a nonlinear analysis to follow. It is a pseudospectral code, periodic in the three spatial Cartesian directions. Such a code is classical[14] and has already been used for similar studies.[15,16] Because the code is fully spectral, it is

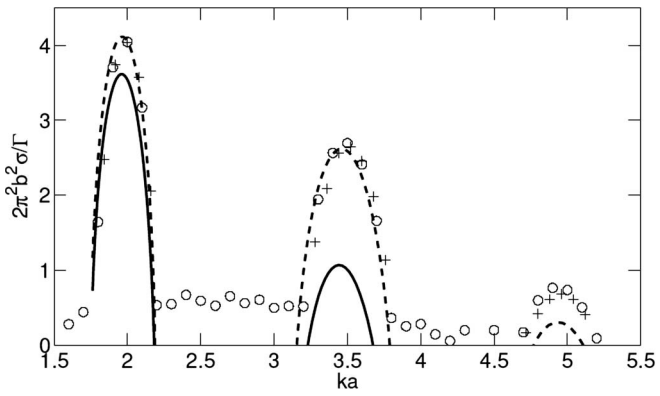

FIG. 1. Comparison of the growth rate computed with the two codes for Re=14 000 and $a/b=0.14$. Circles and crosses are data obtained with the fully spectral code and with the spectral-element code, respectively. Theoretical predictions are in solid line [formula (6.1a) from Le Dizès and Laporte (Ref. 7)] and in dashed line [same formula with a viscous damping term computed by the global approach (see text)].

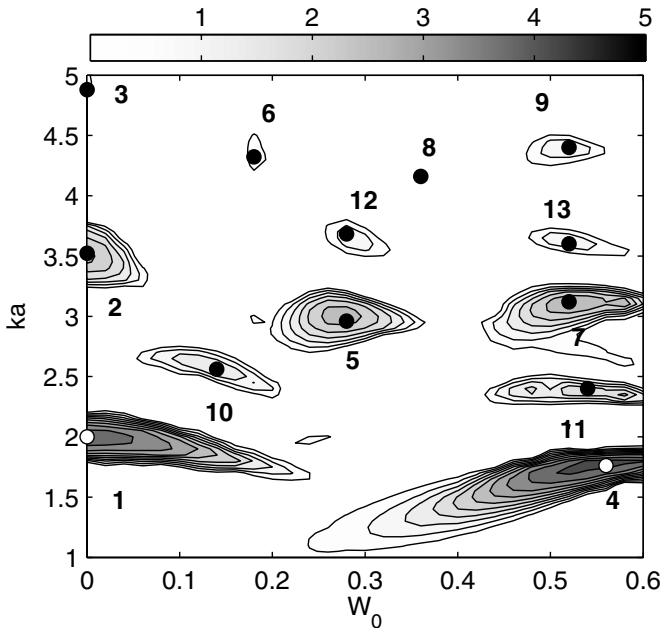

FIG. 2. Contours of instability growth rate in the (W_0, ka) plane for $a/b=0.14$ and Re=14 000. A number has been provided to each important unstable mode and is used hereafter to refer to each of them.

very fast but is in principle limited to flows with zero total circulation.[17] A trick has then to be used to simulate corotating vortex pairs for which the circulation is 2Γ: a solid body rotation $\Omega_0 \mathbf{e_z}$ has to be subtracted from the base flow so that the global circulation at the boundary of the domain is zero.[16] Time integration is performed using an Adams–Bashforth temporal scheme. For determining the 2D base flow, the size L of the square domain has been chosen to be sufficiently large to reduce the influence of image vortices. Typically, we have taken L/b between 5 and 6. A smaller domain with $L'/b \approx 2.5$, centered on the vortex pair, has been taken for the simulation of the perturbation equations. This is possible because the perturbations are localized in the center of each vortex and decrease very fast to zero away from the vortices. Thus, there is no difficulty in considering the perturbations periodic on a smaller domain.

The two numerical codes have been compared and validated for a configuration without axial flow. In Fig. 1 is plotted the growth rate of the perturbations obtained by the two different codes, together with the theoretical formula.[18] As can be seen, the two codes provide the same results for the first three modes. The relative error between the two codes is generally only a few percent. This difference was traced to a slight sensitivity in the growth rate predictions to the time allowed for quasiequilibrium to be reached before freezing the base flow, which was slightly different for the two cases. On the other hand, the large underestimation in the growth rate by the theoretical formula is due to an incorrect estimate of the damping rate associated with viscous effects. In the theory, the damping rate is based on a local approach. If a global estimate is computed using the method of Lacaze *et al.*,[9] the viscous damping is found to be significantly smaller[19] and a much better estimate is obtained. The adjusted theoretical predictions are also shown in this figure by the dashed lines. Note that even this estimate loses accuracy for the higher wavelength mode.

III. RESULTS

A. Mode map

Using the procedure explained above, we have first explored a large part of the parameter space for a fixed Reynolds number Re=14 000 and $a/b=0.14$, with resolution steps for W_0 and k of 0.002 and 0.1, respectively. The growth rate contours of the most unstable modes are displayed in Fig. 2. Only the growth rates (normalized by the turn-over time of the vortex pair) in excess of 0.5 have been indicated in this figure. It demonstrates the existence of several islands of instability. Each island corresponds to a specific instability mode. These modes are localized in the core of each vortex and have the same spatial structure in each vortex. Their spatial structure is shown in Fig. 3. The characteristics of each mode are also provided in Table I.

The first point to note is that the instability map shown in Fig. 2 is very similar to the map obtained for equal strength counter-rotating vortices (see Fig. 11 in Ref. 9). The first three modes, labeled 1–3, which have maximum growth rates for no axial flow but persist for small W_0, are the well-known sinuous modes of the elliptic instability.[5] They correspond to the resonant combination of two Kelvin modes of azimuthal wavenumbers $m=1$ and $m=-1$. Here, the functional dependence of the Kelvin modes is written as $\exp(im\theta+ikz-i\omega t)$, where m and k are the azimuthal and axial wavenumbers and ω is the frequency. Moreover, we assume that k is positive. For $W_0=0$, the sinuous modes are stationary ($\omega=0$) and have been called "principal modes" as they are formed from two Kelvin modes with the same (broad) radial structure. The radial structure of the Kelvin mode can be identified by a label specifying the number of zeros of the radial velocity component of the mode in the vortex core.[9] Principal modes are denoted by (m_1, m_2, n),

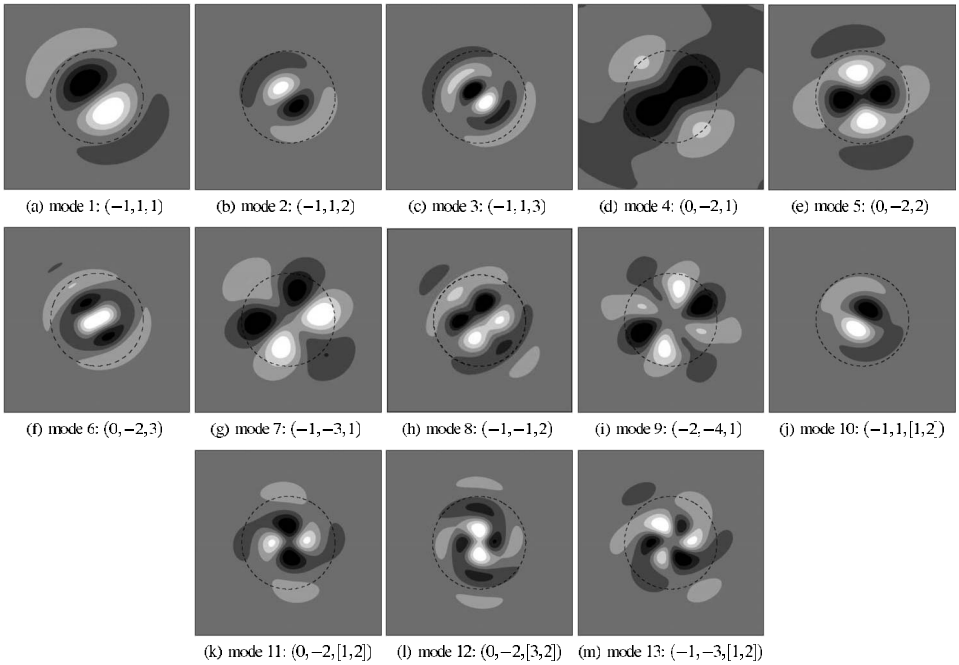

FIG. 3. Axial vorticity perturbation fields resulting from the elliptical instability for Re=14 000 and $a/b=0.14$. Each plot is associated with a number corresponding to one point identified in Fig. 2. Contours are linear and symmetric around 0. The dashed line is a circle of radius a centered on the vortex center.

where m_1 and m_2 are the azimuthal mode numbers of the two resonant Kelvin modes and n is their common (radial) label. It is possible to identify other resonant modes as combinations of Kelvin modes with different radial dependences, in which case the mode is denoted by $(m_1,m_2,[n_1,n_2])$. Examples of these mixed modes can be found in Ref. 9.

Modes 1–3 in Fig. 2 are the principal modes $(-1,1,1)$, $(-1,1,2)$, and $(-1,1,3)$, respectively. Their spatial structures shown in Figs. 3(a)–3(c) have one, two, and three radial oscillations, as indicated by their radial mode numbers. Comparatively to the counter-rotating case, the principal Coriolis effect is to modify the resonance condition, thus shifting the unstable modes toward smaller k, which results in bigger growth rates. For $W_0=0$, the numerical growth rate for these modes is in good agreement with the theory (see Fig. 1). As the axial flow is progressively increased, these modes are progressively stabilized, as also predicted for counter-rotating vortex configurations.[9] As explained by Lacaze *et al.*,[9] this phenomenon has two different causes. First, as soon as an axial flow is present, the symmetry between the $m=1$ modes and the $m=-1$ modes is broken. The resonance between the two helical modes becomes less efficient because their radial structures are no longer perfectly in phase. Moreover, the symmetry breaking creates a small detuning in the resonant frequency with respect to the frequency that maximizes the local instability in the vortex center. Thus, the strength of the local elliptic instability in the vortex center is also less important. The second cause is the damping of the Kelvin mode $m=-1$. The damping of this mode is due to the appearance of a viscous critical layer in its

TABLE I. Parameters of the modes identified in Figs. 2, 6, and 7(a).

			Re=14 000, $a/b=0.14$				Re=14 000, $a/b=0.18$				Re=31 400, $a/b=0.168$			
Mode	m	n	W_0	$2\pi a/\lambda$	$2\pi^2b^2\omega/\Gamma$	$2\pi^2b^2\sigma/\Gamma$	W_0	$2\pi a/\lambda$	$2\pi^2b^2\omega/\Gamma$	$2\pi^2b^2\sigma/\Gamma$	W_0	$2\pi a/\lambda$	$2\pi^2b^2\omega/\Gamma$	$2\pi^2b^2\sigma/\Gamma$
1	−1,1	1	0	2.00	0	4.04	0	1.76	0	5.21	0	1.8	0	5.08
2	−1,1	2	0	3.52	0	2.64	0	3.12	0	4.99	0	3.2	0	4.83
3	−1,1	3	0	4.88	0	0.611	0	4.48	0	4.73	0	4.6	0	4.45
4	0,−2	1	0.56	1.76	−28.8	2.85	0.58	1.68	−15.7	4.81	0.58	1.65	−20.7	4.84
5	0,−2	2	0.28	2.96	−39.1	2.71	0.3	2.88	−20.1	3.74	0.28	2.88	−26.0	4.11
6	0,−2	3	0.18	4.32	−42.3	0.868					0.19	4.11	−27.0	3.39
7	−1,−3	1	0.52	3.12	−84.7	2.88	0.54	3.04	−46.4	3.81	0.55	3	−53.95	4.21
8	−1,−3	2	0.36	4.16	−91.16	0.30					0.37	4.0	−59.8	2.85
9	−2,−4	1	0.52	4.40	−141	1.23					0.53	4.21	−93.6	3.49
10	−1,1	1,2	0.14	2.56	−7.53	1.63	0.1	2.32	−0.59	4.50	0.1	2.4	−0.78	3.42
11	0,−2	1,2	0.54	2.40	−26.3	1.30	0.56	2.24	−15.2	3.06	0.6	2.2	−15.97	3.0
12	0,−2	3,2	0.28	3.68	−37.0	1.21					0.305	3.47	−21.9	3.24
13	−1,−3	1,2	0.52	3.60	−79.1	1.20					0.56	3.4	−48.4	2.84

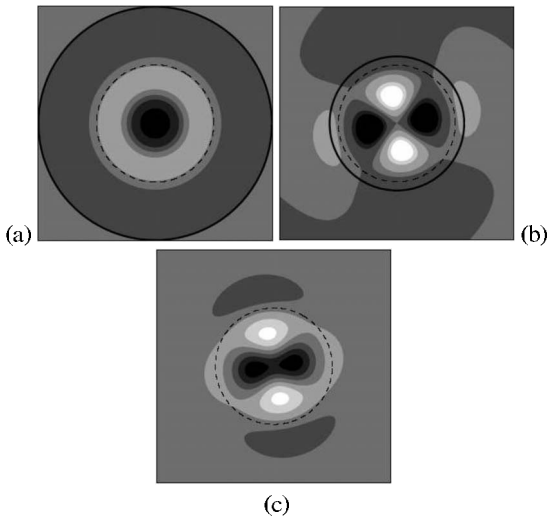

FIG. 4. Azimuthal decomposition of the instability mode 5: axial vorticity in a section perpendicular to the vortex axis. (a) Axisymmetric component ($m=0$), (b) $m=\pm 2$ component, and (c) superimposition of the $m=0$ and $m=\pm 2$ components. The circle (solid line) in (a) and (b) indicates the position of the turning point r_t (see text).

radial structure.[20,21] When the damping rate of the mode is greater than the growth rate associated with the resonance, the instability mode disappears.

The other instability modes that are destabilized for larger values of W_0 are no longer stationary sinuous modes. The mode labeled 5 corresponds to the principal mode $(-2,0,2)$, which has also been observed in the numerical simulation of counter-rotating vortices. This mode is the most unstable for $W_0 \approx 0.3$ and $ka \approx 3$ here. The label of the mode can be obtained by looking at the azimuthal decomposition of the instability mode in one of the vortices, as shown in Fig. 4 for mode 5. Figures 4(a) and 4(b) show the $m=0$ and the $m=\pm 2$ contribution to this instability mode, while Fig. 4(c) is the superimposition of these two contributions alone. We clearly see that the eigenmode shown in Fig. 3(e) is well reproduced, confirming that mode 5 is mainly a combination of the azimuthal wavenumbers $m=0$ and $m=\pm 2$. The time evolution and the three-dimensional structure of the mode, which are shown in Figs. 5(a) and 5(b), respectively, provide further information on the characteristics of the Kelvin modes involved in the construction of mode 5. We observe that the helical structure is right-hand oriented and rotates anticlockwise. This indicates that the axial and azimuthal wavenumbers are of opposite sign, and the frequency and azimuthal wavenumber are of the same sign, thus our choice of positive k, $m=-2$, and $\omega<0$ (as indicated in Table I).

The label n of the Kelvin mode involved in the resonance can be obtained by looking at the radial variation in each azimuthal component. Le Dizès and Lacaze[22] showed that the label corresponds to the number of radial oscillations between the origin and a turning point r_t, which delimits the region where the mode is localized. As explained by Le Dizès and Lacaze,[22] the radial location r_t can be computed from the vortex profile and the characteristics of the mode.

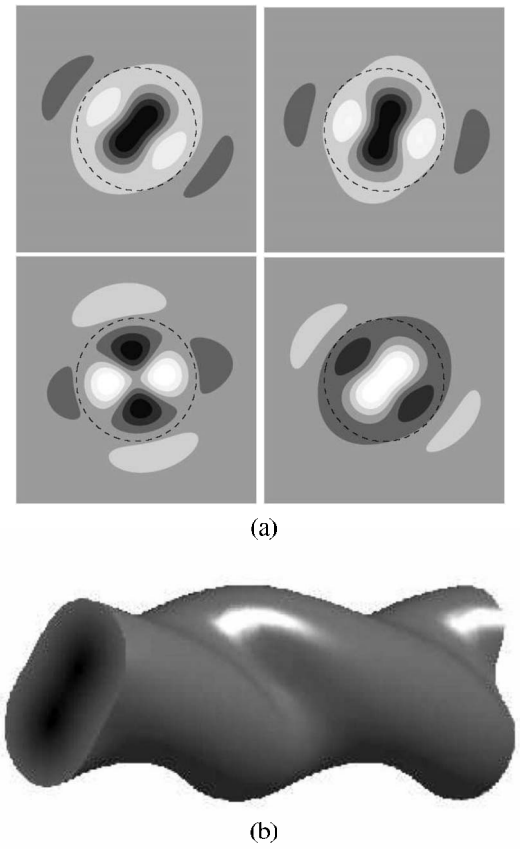

FIG. 5. (a) Temporal evolution of the axial vorticity of the instability mode 5 during half a period. Times correspond to 0, $T/8$, $2T/8$, and $4T/8$, respectively. (b) Three-dimensional visualization showing a vorticity isosurface indicating the deformation induced by mode 5. Here, the maximum vorticity of the instability mode is 0.4 times the maximum vorticity of the base flow.

The turning point r_t has been indicated for the $m=0$ and $m=-2$ components of mode 5 in Figs. 4(a) and 4(b), respectively.

Using a similar azimuthal decomposition and by comparing the figures with the theoretical plot of Lacaze *et al.*,[9] the principal modes $(-2,0,1)$, $(-2,0,3)$, $(-3,-1,1)$, $(-3,-1,2)$, and $(-4,-2,1)$ can be identified with modes 4, 6, 7, 8, and 9 of Fig. 2 (see Fig. 3). Note that an $m=\pm 2$ structure is clearly visible on modes 4 and 6, $m=\pm 3$ structure on modes 7 and 8, and $m=\pm 4$ on mode 9. As expected, the maximum growth rate of the principal modes decreases as their axial wavenumber increases. Other instability modes are also visible in Fig. 2. They are not principal modes, which means that they involve Kelvin modes with different radial labels. A few of them are illustrated in Fig. 3. By looking at the number of oscillations of the main azimuthal components, labels have been tentatively given for each of these modes.

B. Effects of the Reynolds number and vortex separation distance variations

Similar contour plots to Fig. 2 are displayed in Figs. 6 and 7(a) for a/b increasing from 0.14 to 0.18 (closer vortices) and a larger Reynolds number (Re increasing from 14 000 to 31 400), respectively. A corresponding set of insta-

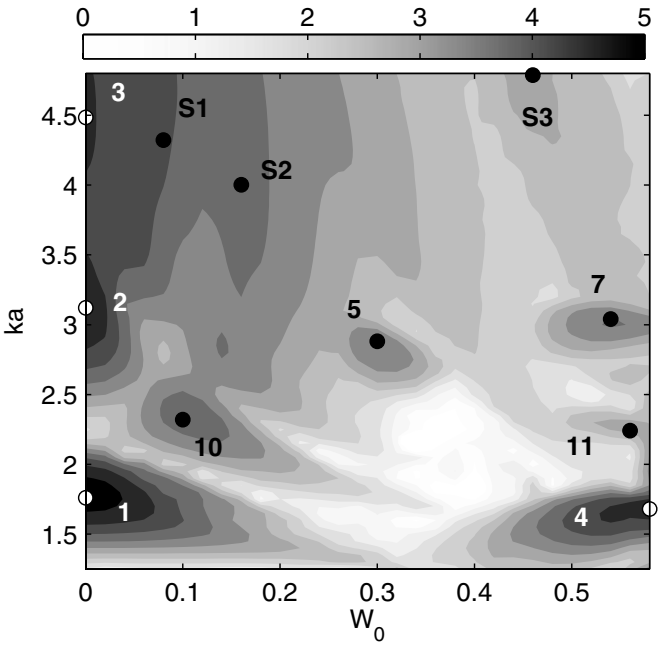

FIG. 6. Same as in Fig. 2 for $a/b=0.18$ and Re=14 000.

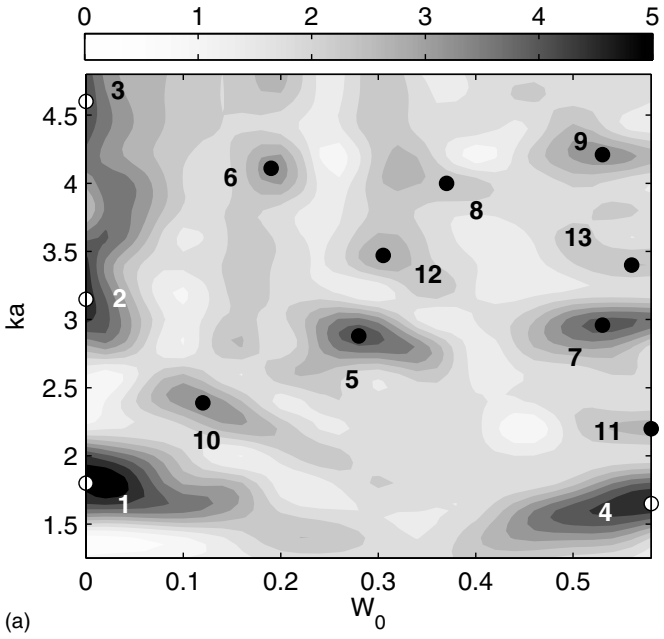

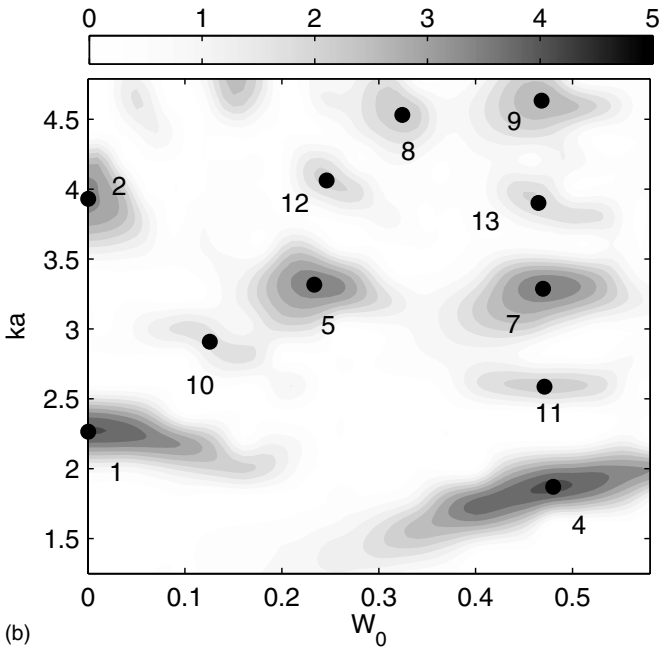

FIG. 7. Same as in for Fig. 2 for $a/b=0.168$ and Re=31 400: (a) corotating vortices; (b) counter-rotating vortices.

bility modes as shown in Fig. 2 can also be identified in these figures. Their characteristics are given in Table I. When a/b is increased, the peaks associated with the main modes move slightly owing to the variation in the mean rotation $2(a/b)^2$ of the pair that modifies the conditions of resonance. In particular, the resonant mode positions are shifted to occur at slightly higher axial flow velocities and smaller wavenumbers. For example, for mode 4, an approximately 30% increase in a/b from 0.14 to 0.18 results in a shift in (ka, W_0) coordinates from (1.76, 0.56) to (1.68, 0.58). The relative shift is not uniform across all modes, however; the 30% change in a/b typically leads to an approximately 10% change in ka but only a few percent change in W_0. The position of the peaks is by contrast almost unaffected by variations in the Reynolds number. This is also clearly seen in Fig. 8(b), where growth rate variations are displayed for a fixed $W_0=0.29$ and for various Reynolds numbers.

An important feature of Figs. 6 and 7(a) is the global increase in the growth rate when either a/b or Re increases. For the range of parameters of these figures, almost the whole parameter space considered is now unstable. However, there are differences between increasing Reynolds number and increasing a/b. When the Reynolds number is increased, the growth rate peaks remain distinct: more modes become unstable, but they can still be identified. Note, in particular, that mode 8, displayed in Fig. 3(h) and which corresponds to the principal mode $(-1,-3,2)$, is now unstable, whereas it was almost stable for the parameters of Fig. 2. When a/b increases, the tendency is different. The peaks of the modes for large ka tend to disappear: the growth rate increases almost uniformly as ka increases. The trend is demonstrated in Fig. 8(a) for a fixed value of $W_0=0.29$ for $a/b=0.18$. In addition, Fig. 9 shows the behavior for the zero axial velocity case. The growth rate ultimately decreases for large ka, but what is important is that there is no dominant mode selection in that case. Again, this is clearly indicated in Fig. 6, which shows that specific modes are virtually indistinguishable from the background noise for $ka \gtrsim 3.5$ for $a/b=0.18$. The modes for $ka \gtrsim 3.5$ are apparently mixed and most of them have a spiral-like structure, as illustrated in Figs. 10(a)–10(c).

The spiral structure is probably associated with a critical layer in one of the resonant modes.[9] This critical layer is known to be responsible for the stabilization of some modes, such as the mode $(-1,1,1)$ for increasing W_0. However, for increasing a/b, this stabilizing effect becomes less important. Moreover, the instability band also becomes wider and the frequency detuning between modes becomes less impor-

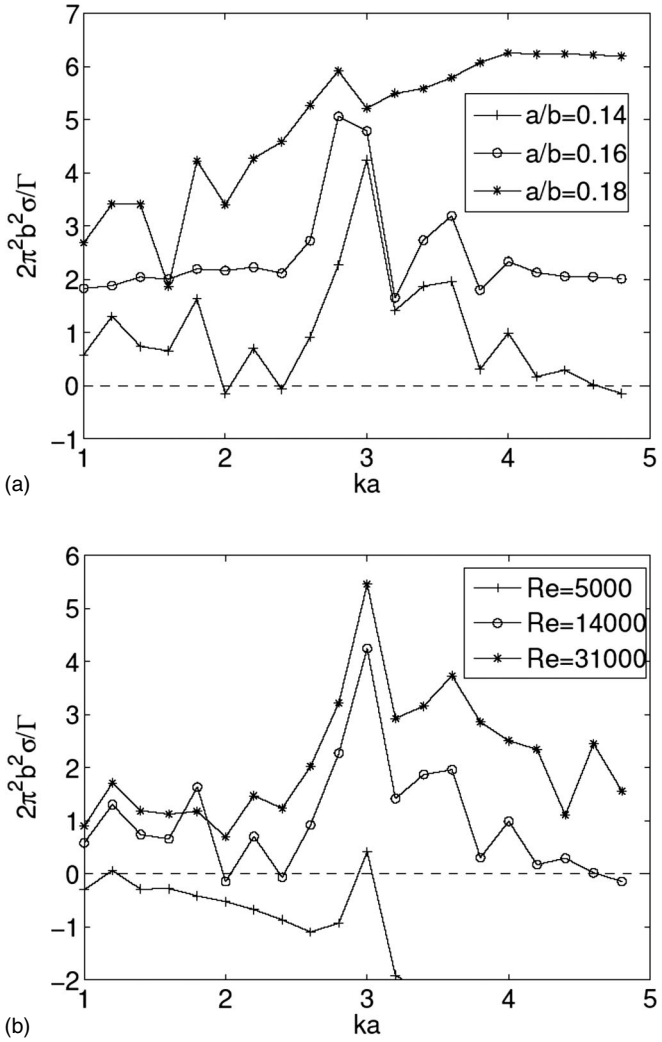

FIG. 8. Instability growth rate vs axial wavenumber for $W_0=0.29$. (a) Vortex separation distance dependence for Re=14 000. (b) Reynolds number dependence for $a/b=0.14$.

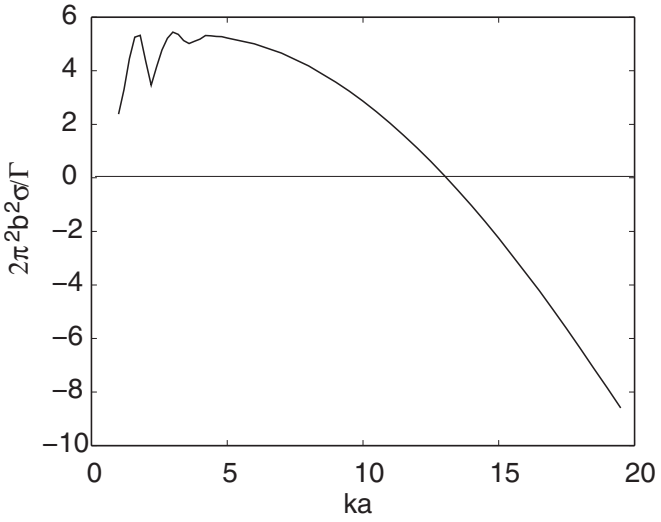

FIG. 9. Growth rate as a function of wavenumber for the corotating case with no axial flow for Re=14 000 and $a/b=0.18$.

tant when a/b grows. Thus, we expect that more and more modes would become unstable in larger and larger overlapping instability regions. The consequence is that the growth rate possesses a large growth envelope with no sharp peaks.

C. Comparison of the stability of co- and counter-rotating vortex pairs

Le Dizès and Laporte[7] compared the dominant instability modes for co- and counter-rotating vortices for the case without axial flow. In general, the growth rates of instabilities for counter-rotating vortices are lower than those for co-rotating vortices and the corresponding wavenumbers of the modes lie between those of the other case. Figure 11 shows growth rate curves for the case without axial flow for $a/b=0.168$ at Re=31 400, which highlights both effects. These predictions are consistent with the analytical and numerical predictions of Le Dizès and Laporte.[7] For the case with axial flow, for which an analytical theory is yet to be developed, Figs. 7(a) and 7(b) display the instability maps for the co- and counter-rotating cases for Re=31 400 and $a/b=0.168$. This allows an explicit, albeit numerical, determination of the effect of the added Coriolis force on the stability of corotating vortex pairs. As previously mentioned, this difference from the counter-rotating case appears because of the mutually induced rotation of the each vortex about their centroid, meaning that they appear quasistationary in a rotating frame.

There are both similarities and differences between the stability maps. The first point is that a similar set of identifiable modes corresponding to the same Kelvin mode interactions appears on each map in roughly the same locations. However, the actual positions of the modes for the corotating vortex map are shifted to approximately 20% higher axial velocities. Another key difference is the background growth rate between identifiable modes. This is very much larger in

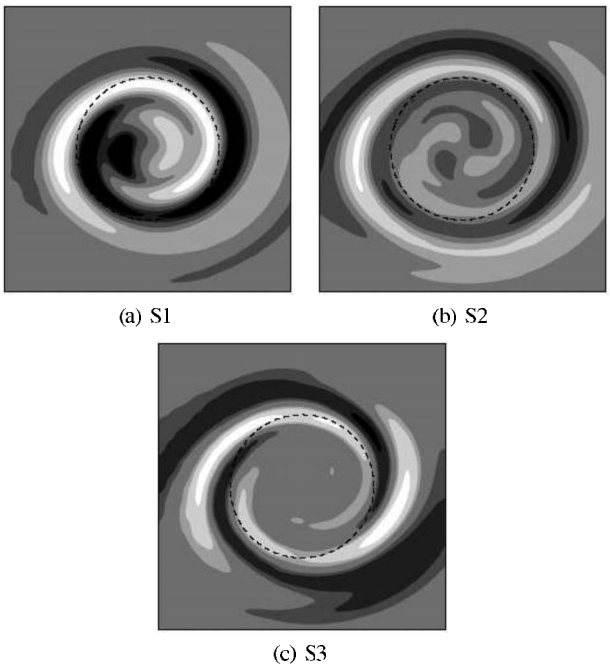

FIG. 10. Instability modes with a critical layer (see Fig. 6).

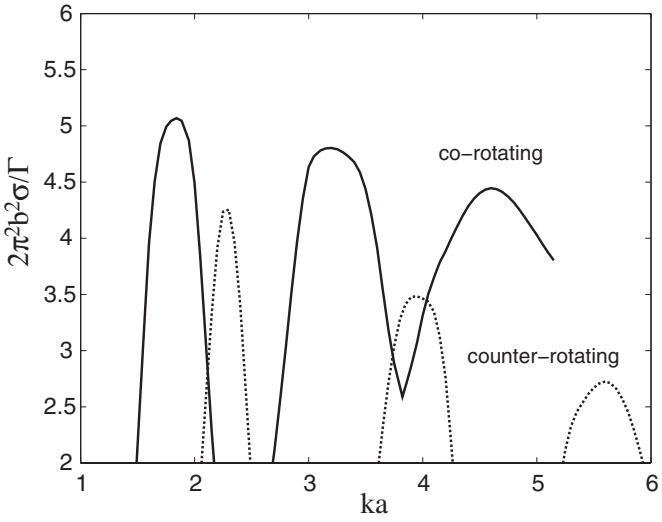

FIG. 11. Comparison of growth rates for equal strength co- and counter-rotating vortices with zero axial velocity for $a/b=0.168$ and Re=31 400.

the corotating case, which is also clear from Fig. 9 at zero axial flow, which explicitly shows the slow falloff of the growth rate for high wavenumbers. Indeed, as discussed in Sec. II, as a/b is increased to 0.18, the background growth rate virtually swamps the growth rate of local resonant Kelvin mode interactions for higher wavenumbers and may even dominate corotating vortex evolution for close vortex cores at particular axial core velocities. This effect occurs at separations well under the merging limit[4] for corotating vortices of $a/b \simeq 0.23$.

IV. CONCLUSIONS

In this work, we have analyzed the linear stability of a corotating vortex pair with axial flow. We have demonstrated that new elliptic instability modes are destabilized by axial flow. For small Reynolds numbers and small a/b, we have shown that the instability diagram resembles the theoretical prediction for counter-rotating vortices,[9] although there are some explicit differences between these cases. When axial flow is progressively increased, the principal modes (combination of Kelvin modes of the same radial branch label) of azimuthal wavenumbers $(-1,1)$ are stabilized and replaced by other principal modes, $(-2,0)$, $(-3,-1)$, and $(-4,-2)$. For large Reynolds numbers or large a/b, other instability modes have been observed and associated with a combination of Kelvin modes with different labels. These other modes are less unstable than the principal modes, whose characteristics are almost invariant, but they make the vortex pair unstable in a large wavenumber band whatever the axial flow. Clearly, it would be interesting to determine the nonlinear evolution of the instability modes and its influence on the merging process.

ACKNOWLEDGMENTS

We would like to thank Thomas Leweke and Kerry Hourigan for discussions and support. We are also grateful to Laurent Lacaze for having computed the theoretical viscous damping used to plot the dashed line in Fig. 1.

[1] Herein, we use this common terminology, although the solution initially obtained by Batchelor (Ref. 23) was the leading order approximation describing the spatial development of far wake trailing line vortices.
[2] P. G. Saffman, *Vortex Dynamics* (Cambridge University Press, Cambridge, England, 1992).
[3] S. Le Dizès and A. Verga, "Viscous interactions of two co-rotating vortices before merging," J. Fluid Mech. **467**, 389 (2002).
[4] P. Meunier, S. Le Dizès, and T. Leweke, "Physics of vortex merging," C. R. Phys. **6**, 431 (2005).
[5] P. Meunier and T. Leweke, "Elliptic instability of a co-rotating vortex pair," J. Fluid Mech. **533**, 125 (2005).
[6] R. R. Kerswell, "Elliptical instability," Annu. Rev. Fluid Mech. **34**, 83 (2002).
[7] S. Le Dizès and F. Laporte, "Theoretical predictions for the elliptical instability in a two-vortex flow," J. Fluid Mech. **471**, 169 (2002).
[8] L. Lacaze, A.-L. Birbaud, and S. Le Dizès, "Elliptic instability in a Rankine vortex with axial flow," Phys. Fluids **17**, 017101 (2005).
[9] L. Lacaze, K. Ryan, and S. Le Dizès, "Elliptic instability in a strained Batchelor vortex," J. Fluid Mech. **577**, 341 (2007).
[10] D. Fabre and L. Jacquin, "Viscous instabilities in trailing vortices at large swirl numbers," J. Fluid Mech. **500**, 239 (2004).
[11] M. C. Thompson, K. Hourigan, and J. Sheridan, "Three-dimensional instabilities in the wake of a circular cylinder," Exp. Therm. Fluid Sci. **12**, 190 (1996).
[12] M. C. Thompson, T. Leweke, and M. Provansal, "Kinematics and dynamics of sphere wake transition," J. Fluids Struct. **15**, 575 (2001).
[13] K. Ryan, M. C. Thompson, and K. Hourigan, "Three-dimensional transition in the wake of elongated bluff bodies," J. Fluid Mech. **538**, 1 (2005).
[14] A. Vincent and M. Meneguzzi, "The spatial structure and statistical properties of homogeneous turbulence," J. Fluid Mech. **225**, 1 (1991).
[15] P. Billant, P. Brancher, and J.-M. Chomaz, "Three-dimensional stability of a vortex pair," Phys. Fluids **11**, 2069 (1999).
[16] P. Otheguy, J.-M. Chomaz, and P. Billant, "Elliptic and zigzag instabilities on co-rotating vertical vortices in a stratified fluid," J. Fluid Mech. **553**, 253 (2006).
[17] D. S. Pradeep and F. Hussain, "Effects of boundary condition in numerical simulations of vortex dynamics," J. Fluid Mech. **516**, 115 (2004).
[18] Note that there is a misprint in formula (6.1a) of Le Dizès and Laporte (Ref. 7): b^2/a_1^2 should be b^4/a_1^4.
[19] L. Lacaze, personal communication (2006).
[20] S. Le Dizès, "Viscous critical-layer analysis of vortex normal modes," Stud. Appl. Math. **112**, 315 (2004).
[21] D. Fabre, D. Sipp, and L. Jacquin, "The Kelvin waves and the singular modes of the Lamb–Oseen vortex," J. Fluid Mech. **551**, 235 (2006).
[22] S. Le Dizès and L. Lacaze, "An asymptotic description of vortex Kelvin modes," J. Fluid Mech. **542**, 69 (2005).
[23] G. K. Batchelor, "Axial flow in trailing line vortices," J. Fluid Mech. **20**, 645 (1964).